JACS
JOURNAL OF THE AMERICAN CHEMICAL SOCIETY
Article
pubs.acs.org/JACS

Superhydrophobic Photosensitizers. Mechanistic Studies of $^1O_2$ Generation in the Plastron and Solid/Liquid Droplet Interface

David Aebisher,*[,†] Dorota Bartusik,[‡] Yang Liu,[§] Yuanyuan Zhao,[§] Mark Barahman,[§] QianFeng Xu,[§] Alan M. Lyons,*[,§] and Alexander Greer*[,‡]

[†]Department of Natural Sciences, Shorter University, Rome, Georgia 30165, United States
[‡]Department of Chemistry, Brooklyn College, City University of New York, Brooklyn, New York 11210, United States
[§]Department of Chemistry, College of Staten Island, City University of New York, Staten Island, New York 10314, United States

Supporting Information

ABSTRACT: We describe here a physical-organic study of the first triphasic superhydrophobic sensitizer for photooxidations in water droplets. Control of synthetic parameters enables the mechanistic study of "borderline" two- and three-phase superhydrophobic sensitizer surfaces where $^1O_2$ is generated in compartments that are wetted, partially wetted, or remain dry in the plastron (i.e., air layer beneath the droplet). The superhydrophobic surface is synthesized by partially embedding silicon phthalocyanine (*Pc*) sensitizing particles to specific locations on polydimethylsiloxane (PDMS) posts printed in a square array (1 mm tall posts on 0.5 mm pitch). In the presence of red light and oxygen, singlet oxygen is formed on the superhydrophobic surface and reacts with 9,10-anthracene dipropionate dianion (**1**) within a freestanding water droplet to produce an endoperoxide in 54−72% yields. Control of the $^1O_2$ chemistry was achieved by the synthesis of superhydrophobic surfaces enriched with *Pc* particles either at the PDMS end-tips or at PDMS post bases. Much of the $^1O_2$ that reacts with anthracene **1** in the droplets was generated by the sensitizer "wetted" at the *Pc* particle/water droplet interface and gave the highest endoperoxide yields. About 20% of the $^1O_2$ can be introduced into the droplet from the plastron. The results indicate that the superhydrophobic sensitizer surface offers a unique system to study $^1O_2$ transfer routes where a balance of gas and liquid contributions of $^1O_2$ is tunable within the same superhydrophobic surface.

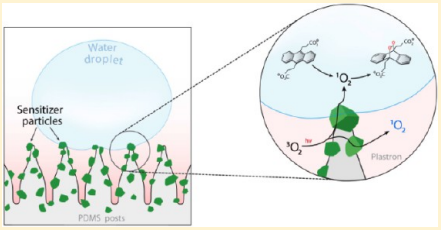

INTRODUCTION

Superhydrophobic surfaces create a unique environment as liquid droplets are poised on the upper portions of the surface features (Figure 1), exposing the liquid surface to the solid/gas interface. The contact angle of aqueous fluids on superhydrophobic surfaces typically exceeds 150°, and the drop can slip off when the surface is tilted less than 10°. The liquid spans between surface features forming a discontinuous liquid/solid interface makes superhydrophobic surfaces fundamentally different from smooth surfaces of the same chemistry. Described in this paper is the study of $^1O_2$ chemistry at superhydrophobic surfaces, which is a new area of investigation (Figure 2). The generation and reactions of $^1O_2$ are of interest from mechanistic and synthetic points of view,[1] but there is a general absence of "borderline" sensitizers in which solvated *or* dry sensitizer sites contribute to $^1O_2$ production in liquids.

A key feature of our superhydrophobic surface is its triphasic character with regions that are controllably dry, partly wetted, or fully wetted. It bears similarity to the work of Rebek et al., where a 3-phase method served for the detection of reactive intermediates (e.g., cyclobutadiene, $^1O_2$, and intermediates in acyl transfer and E1cB reactions) between two solid phases separated by a solution.[2−5] Lahann and co-workers have also made nanocolloids with three unique compartments.[6]

The virtues of superhydrophobic surfaces have been shown, but very few have photocatalytic properties[7,8] or generate reactive oxygen species (ROS). Although superhydrophobic surfaces have been prepared by a variety of techniques,[9,10] fluoro compounds[9−11] and nonfluoro silanes[7] have frequently been used to create hydrophobic TiO_2 surfaces. These films were not robust and lost their superhydrophobicity upon UV irradiation. Hydrothermal techniques to form TiO_2 nanorods[12] and sol-gel and chemical vapor deposition techniques to form TiO_2 nanostrawberry films[13] were used to form superhydrophobic films with reversible wettability. Similarly, nanocomposites of commercially available TiO_2 nanoparticles embedded into a polyethylene surface[14] and a superhydrophobic paper surface created by deposition of TiO_2 nanoparticles using a liquid flame spray process[15] have also been reported with reversible wettability. All of the above TiO_2 films readily become hydrophilic upon exposure to UV light, and their photocatalytic properties have not been reported. In one report, nanocomposite films of TiO_2 dispersed in a polymer matrix were prepared by aerosol-assisted chemical vapor deposition,[16] although the catalyst particles were embedded in the polymer matrix with reduced surface contact area. This

Received: October 14, 2013
Published: December 2, 2013

   dx.doi.org/10.1021/ja410529q | J. Am. Chem. Soc. 2013, 135, 18990−18998

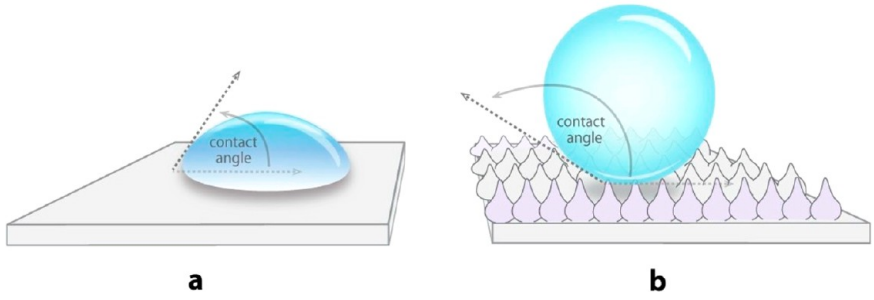

Figure 1. Water drop on a smooth hydrophilic surface (a) and on a rough superhydrophobic surface (b).

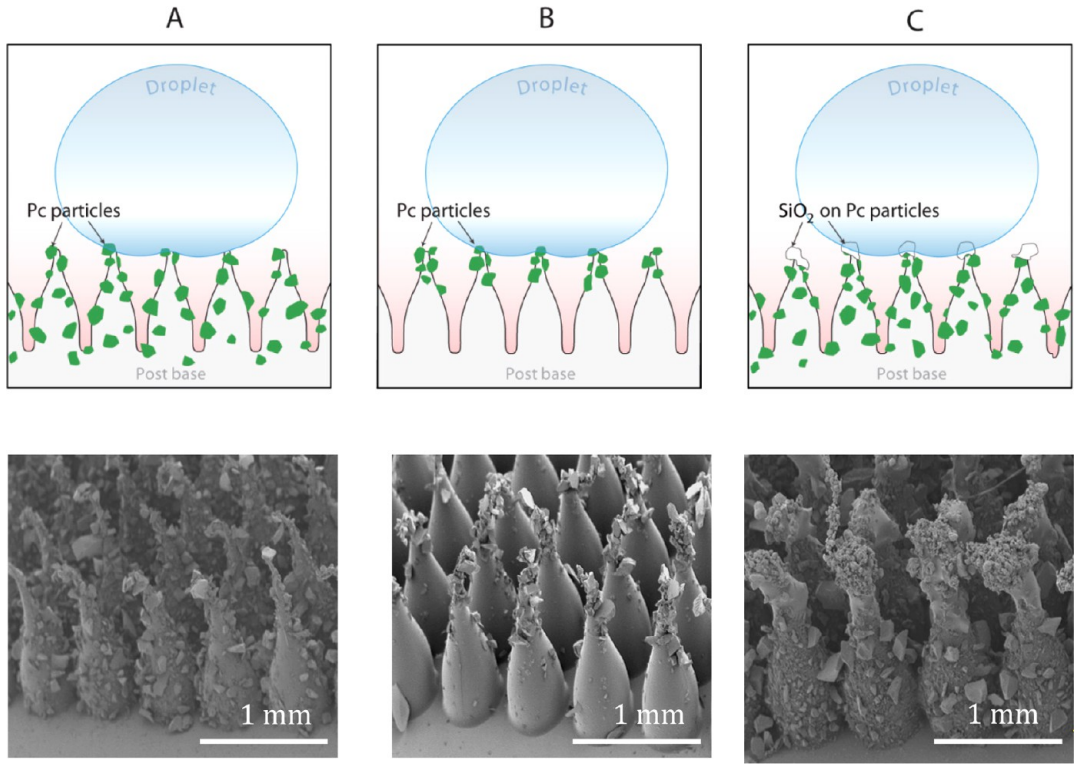

Figure 2. Schematic and SEM images of water droplets on (A) surface A with *Pc* particles uniformly coated on the PDMS posts, (B) surface B with *Pc* particles residing near the tips of the PDMS posts, and (C) surface C with silicone capping the post tips of PDMS posts otherwise uniformly coated with *Pc* particles on the posts. Beneath the "fakir" droplet is the plastron, where the post surfaces remain dry. Here, fakir refers to the droplet's "feat" (as analogous to a person lying on a bed of nails).

surface did photocatalyze the degradation of a dye upon UV illumination, but only when it was fully wetted (Wenzel state, where water completely wets the surface below the droplet, displacing the air residing in between the posts). The kinetics were not reported.

Again, it was of much interest to us that surface wettability could quantifiably affect $^1O_2$ production. We wondered how the mechanism of $^1O_2$ uptake will proceed when it derives from the gas and the aqueous phases. We can mention some attention has been given to polydimethylsiloxane (PDMS) as a solid support. It is often a material of choice for microfluidic experiments,[17] whether to produce small droplets[18,19] or for use in single-molecule fluorescence experiments.[20] PDMS has also been used for stamping in a patterning strategy to control surface wettability at specific sites.[21] At present, superhydrophobic sensitizers represent an undeveloped area. One obstacle is the need for a facile synthesis of superhydrophobic sensitizer solids.

In this regard, we report on the interaction of individual droplets with $^1O_2$ generated from a novel superhydrophobic surface composed of photocatalytic particles partially embedded in printed PDMS posts. High yields of $^1O_2$ in water droplets were quantified by monitoring the decrease in 9,10-anthracene dipropionate dianion, which is selectively oxidized by $^1O_2$. Photolysis of this unique surface with red (669 nm) light generates $^1O_2$ which is trapped in freestanding water droplets on the PDMS surface. No information exists for the requirements for efficient $^1O_2$ capture in water droplets on superhydrophobic surfaces. Thus, surfaces were prepared with the *Pc* particles confined to specific locations in a manner meant to complement each other and help elucidate the relative significance of the $^1O_2$ transport mechanisms from the surface to the droplet: (1) *Pc* particles were uniformly embedded in the PDMS posts (surface A), (2) *Pc* particles were confined to the PDMS postend tips (surface B), and (3) *Pc* particles were embedded in the PDMS posts, but with the postend tips

dx.doi.org/10.1021/ja410529q | J. Am. Chem. Soc. 2013, 135, 18990−18998

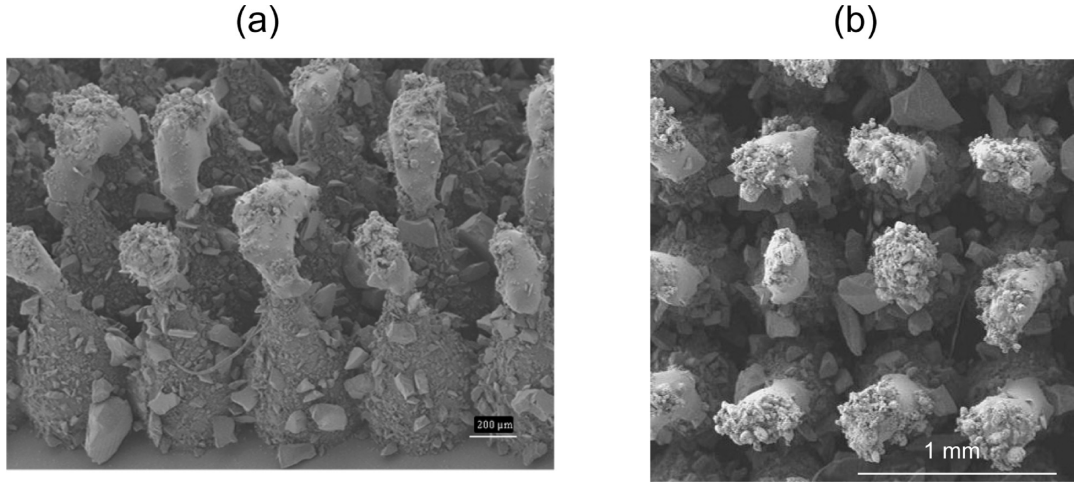

Figure 3. Oblique (a) and aerial (b) SEM views of surface C. The post tips are coated with an extra layer of PDMS embedded with agglomerates of silica nanoparticles. Larger *Pc* particles (25−200 μm) coat the majority of the post surface.

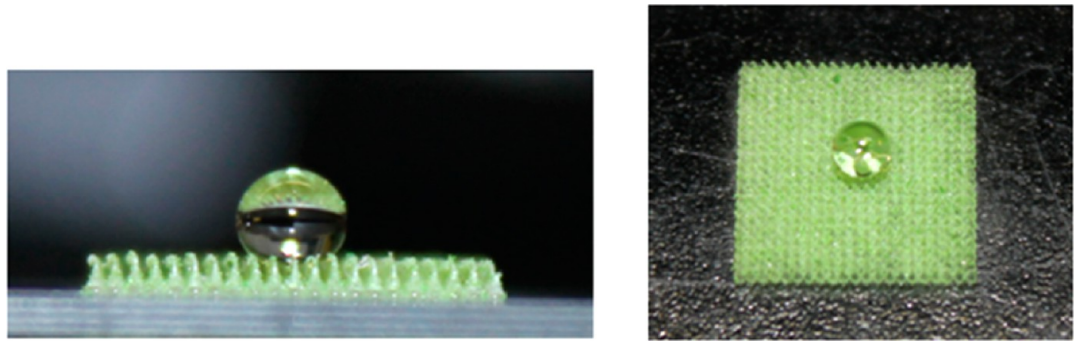

Figure 4. Side and aerial photographic views of a 10-μL water droplet on surface A.

Table 1. Parameters of Superhydrophobic Surfaces A−C

droplet volume (μL)	contact angle (deg) of surfaces A−C[a,b]	measured diameter of droplet (largest width) on surface A (mm)	calculated diameter of ideal spherical drop (mm)	% increase from a perfect sphere	length of droplet contact on surface A (mm)[a]	# of post tips in contact with drop along diameter on surface A	% evaporation of droplet after 1 h
10 ± 2	163.6 ± 3.2	2.74 ± 0.01	2.7	1.5%	1.45 ± 0.02	3−4	60%
20 ± 2	163.3 ± 3.4	3.58 ± 0.01	3.4	5.3%	2.29 ± 0.05	5	30%
25 ± 2	163.8 ± 2.8	3.86 ± 0.01	3.6	7.2%	2.37 ± 0.02	5	30%
30 ± 2	161.6 ± 3.6	4.16 ± 0.01	3.9	6.7%	2.76 ± 0.02	6	20%
40 ± 2	159.8 ± 3.3	4.76 ± 0.01	4.2	13%	3.38 ± 0.01	7	15%
50 ± 2	158.4 ± 3.6	5.07 ± 0.01	4.6	10%	3.42 ± 0.01	7	12%
60 ± 2	159.0 ± 3.1	5.48 ± 0.01	4.9	12%	3.91 ± 0.01	8	10%
70 ± 2	157.0 ± 3.0	5.77 ± 0.01	5.1	13%	4.41 ± 0.03	9	7%
80 ± 2	157.1 ± 4.0	6.01 ± 0.01	5.3	13%	4.72 ± 0.03	10	6%
90 ± 2	156.8 ± 2.1	6.34 ± 0.01	5.6	13%	4.85 ± 0.01	10	5%
100 ± 2	156.1 ± 2.9	6.53 ± 0.01	5.8	13%	5.32 ± 0.02	11	5%

[a]The values shown here are an average of 2 or more measurements. [b]Even though surface C is coated with a silicone "tip" and differs from the *Pc* particle tips of surfaces A and B, contact angles were all within experimental error of each other for any given droplet volume.

capped with silicone so that no *Pc* particles could contact the droplet itself (surface C) (Figure 2).

Analysis of the three PDMS surfaces gives mechanistic insight into the factors determining $^1O_2$ capture within the water droplets via sensitization of $^3O_2$ at dry *or* wet excited *Pc* sites on the superhydrophobic surfaces. Such superhydrophobic $^1O_2$-generating surfaces may prove useful for applications in "green" photooxidations.

RESULTS AND DISCUSION

Photosensitizer-Embedded Superhydrophobic Surfaces A−C. The printing of the PDMS post surfaces was carried out as reported previously.[22] PDMS surfaces were printed in 1 cm^2 square (20 × 20) arrays with a pitch of 0.5 mm. Singlet oxygen-generating silicon phthalocyanine (*Pc*) glass was prepared as previously described.[23] The glass was ground to particles 25−200 μm in diameter and spread onto the PDMS surface immediately after printing. The surfaces were then

dx.doi.org/10.1021/ja410529q | J. Am. Chem. Soc. 2013, 135, 18990−18998

cured at 65 °C for 2 h. Unattached *Pc* particles were removed by exposing the surface to high flows of compressed air. On average, 19 ± 3 mg of *Pc* particles were embedded into the 20 × 20 post array surface (4.8 ± 1 × 10^{-5} g of *Pc*/post). Assuming an average particle diameter of 100 μm, the average number of particles per PDMS post would be 69 ± 11 particles/post.

For surface A, *Pc* particles were spread uniformly over the entire surface. For surface B, *Pc* particles were predominately confined to the PDMS postend tips. For surface C, post tips were capped with silicone (Corning 3140) that was subsequently coated with silica nanoparticles (Cabot TS-530). This was achieved by dipping a surface prepared as per sample A (with a uniform distribution of *Pc* particles) into a thin layer of uncured silicone. After coating the tips with PDMS, the surface was dusted with silica nanoparticles before cure. Although the *Pc* particles at the tips were coated with silicone, the majority of the *Pc* particles remained exposed along the PDMS posts in the plastron (Figure 3).

Freestanding Water Droplets. Water droplets were dispensed gently onto surfaces A−C from a height of ∼1 mm with little to no momentum upon impact. Any significant momentum would increase the surface contact line compared to drops placed gently on the surface. Figure 4 shows a 25 μL water droplet on surface A. Clearly, the water droplets on surfaces A−C showed Cassie−Baxter behavior (drop sits on the posts with air underneath);[24] there was no wetting of the post interstices (i.e., Wenzel state),[25] which can occur on other types of rough surfaces.[26,27] In our case, droplet volumes ranged from 10 to 100 μL; larger droplet volumes led to small contact angle decreases from 163.6° to 156.1° (Table 1) Figure 5A shows that the 10 μL droplet is mostly spherical. Figure 5B shows an example of the ellipsoidal shape of the larger 100 μL droplet due to the effects of gravity. The standard deviation of the droplet diameter is ±0.01 mm.

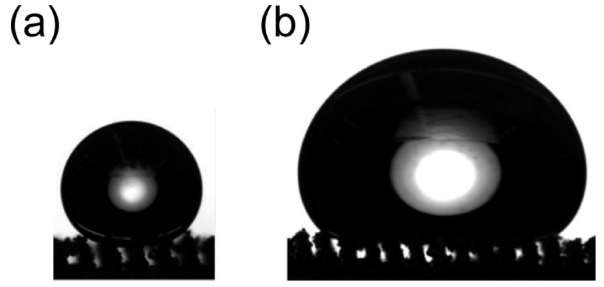

Figure 5. Optical images of surface A and a water droplet of a 10 μL volume (a) and a 100 μL volume (b).

Table 1 also shows the diameter of the droplet both at its widest point and at the calculated diameter of ideal spherical drops. The percent increase in droplet diameter over a perfect sphere of the same volume is shown. As the droplet volume increases, the percent increase in diameter increases, and the structure becomes oblong in shape. Below 40 μL, the measured diameter begins to approach the diameter expected for a perfect sphere. The largest diameter was measured with good precision, but the contact length along the surface becomes less precise as it is difficult to identify the intersection between air, droplet, and surface.

An estimate of the number of posts in contact with a droplet, along the contact diameter, is also shown in Table 1. The total number of posts in contact with the droplet could not be determined precisely as there are some posts, close to the contact line, that may be partially wetted by the droplet, depending upon the details of how the droplet contacts the surface. Notice that the number of contact posts along the diameter does not increase linearly with drop volume. In some cases, the number of contact posts is the same for two drops of different volume. This occurs because the contact line is discontinuous, and so "jumps" in the contact line length occur. This phenomenon has been observed previously for superhydrophobic surfaces composed of uniform arrays of posts.[22]

The total number of posts in contact with the droplet is shown in Table 2. This value was estimated using three droplet volumes (10, 25, and 60 μL) by applying a water droplet containing rhodamine B dye onto a surface prepared using TiO_2 nanoparticles (in place of *Pc* particles); the dye is absorbed on the TiO_2 surface. In this way, we observe an otherwise difficult feature to quantify, the degree of post wetting. After removing the droplet, posts contacting the droplet fully or partially can be counted under an optical microscope (Figure 6, where fully wetted inner posts are counted as 1 and partially wetted outer posts are counted as 0.5) and compared to a geometrical model based on the observed contact diameter (Supporting Information Figure S13 and Table S1). For surfaces A−C, the estimated number of post tips in contact with the water droplets ranged from 7 (for the 10 μL droplet) to 93 (for the 100 μL droplet). For surface A, this would correspond to a mass of *Pc* particles ranging from 0.35 to 4.6 mg. Because the water droplet is in contact only with the top of each post, less than 10% of the particles are in

Table 2. Photooxidation of Anthracene 1 Within H_2O Droplets

droplet volume (μL)	% yield of **2** with surface A	% yield of **2** with surface B	% yieldof **2** with surface C	# of post tips in contact with drop	wetted Posts:droplet volume ratio (posts/μL)
10 ± 2	72 ± 43	54 ± 32	13 ± 8	7−12	0.7−1.2
20 ± 2	68 ± 20	52 ± 16	12 ± 4	21	1.1
25 ± 2	70 ± 21	51 ± 15	13 ± 4	21	0.8
30 ± 2	69 ± 14	52 ± 10	13 ± 3	30	1.0
40 ± 2	65 ± 10	50 ± 8	12 ± 2	41	1.0
50 ± 2	59 ± 7	46 ± 6	11 ± 1	41	0.8
60 ± 2	53 ± 4	40 ± 4	10 ± 1	48	0.8
70 ± 2	52 ± 4	39 ± 6	9.8 ± 0.7	63	0.9
80 ± 2	51 ± 4	40 ± 4	9.6 ± 0.7	74	0.9
90 ± 2	52 ± 3	39 ± 5	9.8 ± 0.5	74	0.8
100 ± 2	54 ± 4	41 ± 6	10.2 ± 0.7	93	0.9

dx.doi.org/10.1021/ja410529q | J. Am. Chem. Soc. 2013, 135, 18990−18998

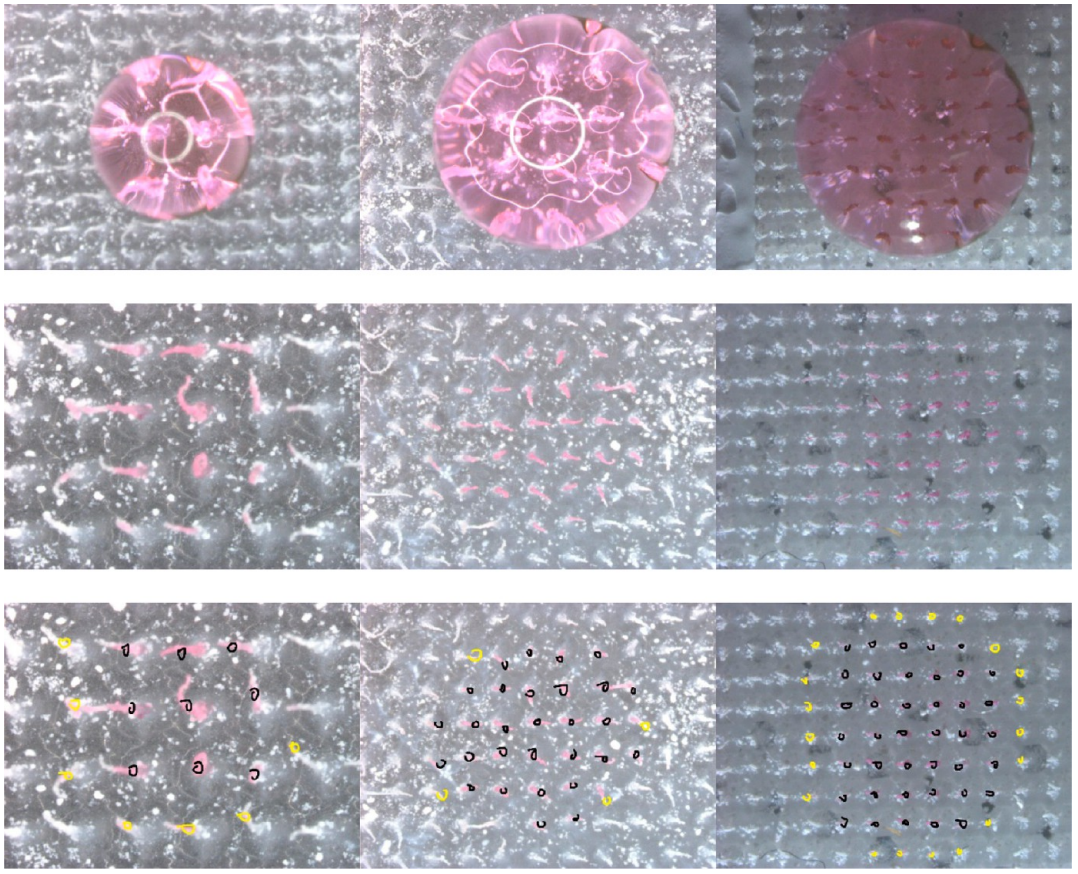

Figure 6. Measurement of the number of posts contacting the water droplet by staining from droplets containing rhodamine B dye on a TiO_2–PDMS post surface. Dark color, inner posts are counted as 1 (marked with black); light color, outer posts are counted as 0.5 (marked with yellow).

direct contact with the liquid drop, leaving >90% of the particles in the air layer under the droplet (plastron). For surface C, no *Pc* particles are in direct contact with water as the post tips are coated with silicone; however, a similar number of particles are in the air layer under the droplet as for sample A.

Droplet Evaporation. The dependence of the evaporation rate on the water droplet volume is shown in Table 1. Smaller droplets evaporated faster, as a percentage of their total volume, as has been reported before,[28,29] because of their greater surface to mass ratio. For example, the 10 μL droplet was found to evaporate 3.2 times faster than the 50 μL droplet (Figure 7). The 10 and 20 μL droplets posed a difficulty in handling; they readily slipped off the PDMS surfaces due their low mass and low air resistance.[30,31] All droplets, regardless of size, easily rolled off the PDMS surfaces upon tilting the surfaces, as would be expected of a superhydrophobic surface with low contact angle hysteresis (facile rolling due to the small number of liquid/solid contact points).[32,33] It is this high mobility of the droplet that enables the facile removal of the drop from the surface and its subsequent analysis by UV–vis spectroscopy.

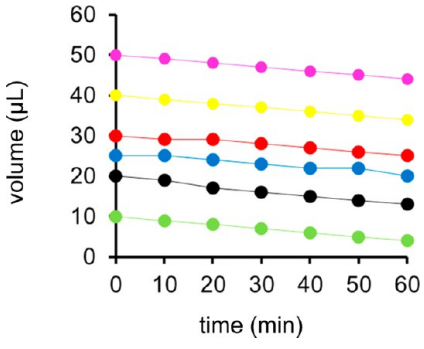

Figure 7. Water droplet evaporation as a function of time on a 1 × 1 cm^2 piece of surface A while being irradiated at 669 nm. The laser light exited the fiber optic and was positioned below surface A.

Effect of Surface Type on Product Yield. Singlet oxygen generated by surfaces A–C upon illumination at 669 nm was detected by its reaction with 9,10-anthracene dipropionate dianion (**1**) (Scheme 1). Singlet oxygen only reacts with **1** to yield **2**, and in view of the ease of monitoring $^1O_2$ trapping by **1** in water,[34] it served as a good chemical probe for $^1O_2$ capture in the H_2O droplets. Irradiation of **1** in a 25 μL H_2O droplet on a native PDMS surface, which had no *Pc* particles, did not produce endoperoxide **2** or other products. Though release-and-capture mechanisms are well established in some

Scheme 1

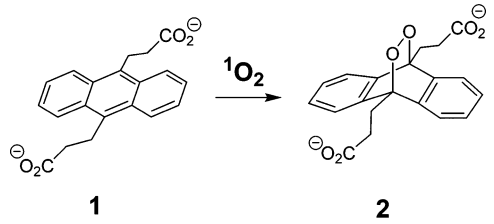

dx.doi.org/10.1021/ja410529q | J. Am. Chem. Soc. 2013, 135, 18990–18998

heterogeneous catalysts,[35,36] they were not of concern here because the *Pc* catalyst was covalently bound to the particles.

As shown in Table 2, the percent yield of **2** from photolysis of surface A is near the sum of the yields of **2** from surfaces B and C. This result shows that the *Pc* particles that are in contact with the droplet, as well as those isolated in the plastron, both contribute to the formation of singlet oxygen and are both trapped within the droplet. Combining the two types of particles creates an additive increase in the concentration of trapped $^1O_2$. The results also clearly show that trapping rate of $^1O_2$ in the droplet from wetted *Pc* particles is enhanced compared to trapping of $^1O_2$ generated in the plastron from dry *Pc* particles.

Table 2 also shows that for surfaces A–C, the percent yields of **2** are similar for the small and large water droplets to within experimental error. A known facet of $^1O_2$ is its short ~150 nm diffusion distance in H_2O,[37] which would restrict its ability to travel deep into the droplet. Because of this short $^1O_2$ diffusion length, the contact area between droplet and surface (i.e., the ratio of the number of posts in contact with the droplet to droplet volume), rather than the droplet volume alone, should be expected to affect the percent yield of **2**. Even if D_2O was used, the longer diffusion length (about 2.8 μm)[1] would only be 1% of the droplet height. Because the height of the droplet, regardless of droplet diameter, is much greater than the diffusion length, it would not be expected to affect the results. It would be expected that the yield of **2** will track linearly with the number of posts in contact with the droplet (and thus the number of particles wetted by the droplet). The mean ratio of wetted posts: droplet volume is 0.9 ± 0.1. For the 10 μL drop, this ratio is highly dependent on the size of the droplet and can range from 0.7 to 1.2 depending on a small change in droplet-surface contact area as shown in the last column of Table 2. To within experimental error, we observe a similar % yield for the small and large droplets.

These results are subject to some experimental error, the largest of which was the evaporation of water over the course of the experiments. After 1 h of photolysis, significant evaporation of the 10 μL droplet was observed (60% decrease in initial volume) but was less significant for the 100 μL droplet (5%). Evaporation reduces droplet size, and so the number of particles in contact would also decrease. The reduced liquid–*Pc* particle contact would be expected to suppress the yield of **2**; however, the concentration of **1** will increase with evaporation of water, leading to an acceleration of the rate, which could compensate for the decreased postdroplet contact. High evaporation rates could also increase convection within the droplet, further enhancing the effective concentration of **1** near the wetted *Pc* particles, leading to an increased rate of formation of **2**. Mixing in small droplets is known to be diffusion limited when droplet volume is stable, and there was no convection within the droplet.

An added way to gain information concerning the water droplet $^1O_2$ chemistry is by following the kinetics for the disappearance of **1**. The rate of disappearance of anthracene **1** as well as a calculation of the number of moles and concentration of endoperoxide **2** is shown in Table 3. Table 4 shows the k_{obs} values obtained from slopes of first-order plots for surfaces A–C. Plots of ln [**1**] vs time showed the first-order disappearance of **1** for surfaces A and B, but not for C (Supporting Information Figure S3). We found that the rate constants for surfaces A and B were similar, which provides evidence for similar mechanisms. Using the reported $^1O_2$ chemical quenching rate of **1** (k_r = 8.2 × 10^7 M^{-1} s^{-1}),[38] we calculate a $^1O_2$ steady state concentration of 8.5 × 10^{-12} M and 7.0 × 10^{-12} M for surfaces A and B, respectively. Such steady state $^1O_2$ concentrations are similar to that found by Haag and Hoigné[39] for a heterogeneous sensitizer $[^1O_2]_{ss}$ = 8 × 10^{-12} M for furfuryl alcohol photooxidation in water. Different kinetics are observed for surface C, where a first-order plot resulted in a low R^2 value of 0.361. This is consistent with the additional mechanisms involved: the transport of $^1O_2$ from the plastron to the droplet surface and solvation of $^1O_2$ by water before $^1O_2$ can diffuse through the solution and react with **1**. Singlet oxygen is known to be highly sensitive to local environments, such as variable access to tryptophan sites in proteins that have a pronounced effect on the reaction rate of $^1O_2$[40] as well as protein dynamics[41] and site of generation.[42,43]

Table 3. Rate of Endoperoxide 2 Formed in a 25 μL Water Droplet[a]

sample	rate (nmol/min)	number of moles of **2** (nmol) formed[b]	concentration of **2** (mM) formed[b]
surface A	0.080	4.8	0.19
surface B	0.067	4.0	0.16
surface C	0.015	0.9	0.036
native PDMS	n/a	0	0

[a]An error of 8% was introduced by the use of a syringe to introduce 25 μL drop onto the surfaces. [b]Data were not corrected for the 30% droplet evaporation that occurred over 1 h.

Table 4. First Order Rate Constants and Steady-State Singlet Oxygen Concentrations from the Photooxidation of Anthracene 1 in 25 μL Water Droplets[a]

experiment	$k \times 10^{-4}$ (s^{-1})	R^2	$[^1O_2]_{ss}$ (M)
surface A	0.71	0.997	8.5 × 10^{-12}
surface B	0.47	0.970	7.0 × 10^{-12}
surface C	[b]	[b]	[b]
native PDMS	n/a	n/a	n/a

[a]An error of 8% was introduced by the use of a syringe to introduce 25 μL drop onto the surfaces. [b]The data for surface C does not fit to first-order kinetics.

Plastron and Liquid Phase Singlet Oxygen Mechanisms. The mechanisms of endoperoxidation of **1** are proposed to proceed as shown in Figure 8. Excited *Pc* particles in contact with the liquid droplet can sensitize solvated $^3O_2$ to $^1O_2$ (Figure 8A) concurrent with dry excited *Pc* particles for gas phase $^1O_2$ generation in the plastron (Figure 8B). The oxidation of **1** then proceeds from uptake of $^1O_2$ where it originated mutually from aqueous *and* gas phases. Evidence suggests that $^1O_2$ generated in the plastron phase migrates into the water droplet but that this route is less efficient. Table 3 shows the rate of formation of endoperoxide **2** in a 25 μL droplet was 0.080 nmol/min for surface A, 0.067 nmol/min for surface B, and 0.015 nmol/min for surface C. This is a ~5-fold reduced rate of formation of **2** for surface C compared to surfaces A and B. There are no *Pc* particles in contact with the aqueous phase on surface C because the post tips are capped with silicone. Thus, we can estimate that ~20% of the singlet oxygen trapped in a 25 uL droplet is generated in the gas phase of the plastron of surface A, whereas ~80% of the trapped $^1O_2$ is formed in the aqueous phase from wetted *Pc* particles in contact with the droplet. Because <10% of the particles under a

dx.doi.org/10.1021/ja410529q | J. Am. Chem. Soc. 2013, 135, 18990–18998

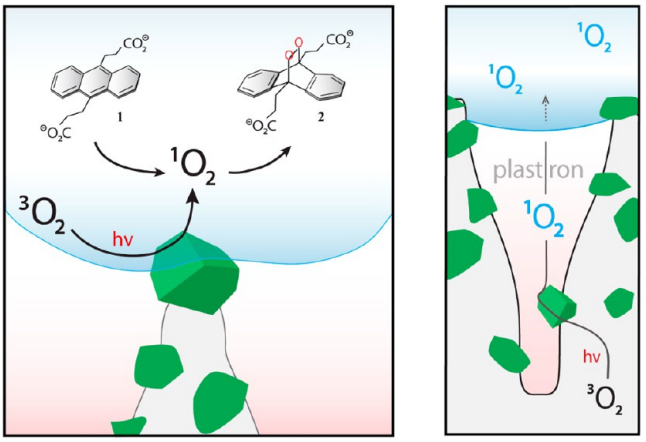

Figure 8. Proposed H_2O droplet photooxidation mechanism. Solvated $^1O_2$ is generated from wetted *Pc* particles in the droplet (A), and gas phase $^1O_2$ is generated from dry *Pc* particles in the plastron that reside under the droplet with less efficient mass transfer of $^1O_2$ into the liquid phase (B).

droplet are in contact with the liquid (>90% remain dry in the plastron layer), the relative efficiency of wetted vs dry *Pc* particles is >45. However, the presence of efficient excited-triplet-state quenchers[44] in the droplet itself would have no affect on the plastron-derived $^1O_2$, which is an interesting control feature. Once singlet oxygen is solvated in the droplet it would be subject to the same quenchers. Other airborne $^1O_2$ reactions have been useful for reactions at solid surfaces. In this regard, Majima et al. reported on $^1O_2$ detection at a TiO_2 surface,[45,46] and Linker et al. were successful in using air-borne $^1O_2$ with thin films of diphenylanthracene as a lithographic technique.[47]

In the course of our research, we developed a method to introduce singlet oxygen via gas bubbles into water avoiding direct contact of the liquid with the sensitizer particles.[23,48] Surface C provides similar functionality as such a singlet oxygen generator. Dry *Pc* particles alone, physically removed from the liquid, lead to the generation of singlet oxygen and its diffusion into the liquid droplet. Although the rate is relatively low compared to wetted sensitizer particles, this approach may still prove useful for generating singlet oxygen in solution while avoiding direct sensitizer-liquid contact.

■ CONCLUSION

We report on the interaction of individual droplets with $^1O_2$ generated from a novel superhydrophobic surface composed of photocatalytic particles partially embedded in printed PDMS posts. The sensitizing *Pc* particles were confined to specific locations on the PDMS posts to obtain mechanistic insight into the transport of $^1O_2$ generated from compartments that are wetted or remain dry in the plastron. Thus, the mechanisms for oxygen uptake to **1** were examined where $^1O_2$ was selectively generated in the aqueous or gas phases.

When the *Pc* particles are wetted by the droplet, singlet oxygen reacts rapidly with **1**, and the reaction follows the expected first order kinetics. By separating the *Pc* particles from the droplet, a change in the photooxidation mechanism was observed as $^1O_2$ produced in the plastron must diffuse to the droplet surface and become solvated before it can react with **1**. Within the water droplet, $^1O_2$ is trapped by anthracene **1** more efficiently by a 5:1 ratio when it was generated by sensitization of $^3O_2$ dissolved in water at the *Pc* particle/droplet interface than at the *Pc* particle/plastron interface. Given that >90% of the particles under the droplet remain dry in the plastron layer, the relative efficiency, calculated on a sensitizer particle basis, may exceed 45:1.

When generated in the plastron, two mechanisms would limit the probability of $^1O_2$ reacting with **1**. First, it is more likely that $^1O_2$ would diffuse away from, rather than toward the droplet surface. As a result, most of the $^1O_2$ generated in the plastron would not enter the droplet. Second, the time required for the molecule to diffuse from the particle surface to the liquid surface and the subsequent solvation of $^1O_2$ would reduce the lifetime of $^1O_2$ in the droplet. However, the approach has benefits that can outweigh lower efficiency. This new class of triphasic system that is capable of isolating sensitizer particles in regionally wet or dry compartments can help address problems in the disinfection of water or wounds as well as provide insights into heterogeneous organic photo-oxidations when the direct contact of the solution with a sensitizer is problematic. Further research is needed to understand the impact of catalyst-solution proximity and wetting on photooxidation reactions. In addition, the effect of convection within the droplet on photooxidation rate will be the topic of future studies. Future work could also examine the reactivity of compounds with a preference for residence in bulk droplet vs outer surface, as for example has been computed recently for small droplets with MD simulations.[49] Further insight into the superhydrophobic $^1O_2$-generating surfaces described in this paper may have relevance to flow[50,51] and bubble reactor[52] applications for "green" photooxidations.

■ EXPERIMENTAL SECTION

Reagents, Materials, and Instrumentation. Silicon phthalocyanine dichloride ($SiPcCl_2$), 3-aminopropyltriethoxysilane (ATPS), 3-glycidyloxypropyl-trimethoxysilane (GPTMS), polydimethylsiloxane, 9,10-anthracene dipropionic acid, and sodium hydroxide were purchased from Sigma-Aldrich (Allentown, PA). Corning 3140 silicone was purchased from Dow Corning Corporation (Midland, MI). The gold (Au) and platinum (Pt) 60/40 for SEM images was purchased from Electron Microscopy Sciences (Hatfield, PA). The above chemicals were used as received without further purification. Deionized water was purified using a U.S. Filter Corporation deionization system (Vineland, NJ). UV−vis spectra in H_2O were collected with Hitachi U-2001 or Shimadzu-1800 spectrophotometers. Images of surfaces A−C were acquired with an AMRAY 1910 Field Emission Scanning Electron microscope (SEM). A ràme-hart Instrument Co. model 250 goniometer (Succasunna, NJ) was used with Image-Pro software to measure contact angles and droplet diameters.

Irradiation Procedure. The light source was a 669 nm diode laser (383 mW) (Model 7404, Intense, North Brunswick, NJ). The 669 nm laser selected as the output wavelength matches the Q-band absorption of the *Pc* particles at 670 nm. The laser optical energy was directed through a multimode FT-400-EMT optical fiber (numerical aperture 0.39; 0.4 μm core diameter × 3 ft length, Thorlabs, Newton, NJ) toward the bottom of a 1 mm thick glass slide that supported the PDMS surface. The distance between the fiber optic head and the glass slide was 5 mm. With a divergence angle of 32°, the 1 cm^2 square PDMS surface was nearly uniformly illuminated with the 669 nm light. Analysis of the water samples after photolysis indicated that no *Pc* particles had dislodged from the PDMS

dx.doi.org/10.1021/ja410529q | J. Am. Chem. Soc. 2013, 135, 18990−18998

surface and relocated into the water droplets. The droplet evaporation experiments were carried out at 26 °C (fluence rate = 1746 J/cm^2), where images were recorded before and after the 1 h irradiation period. The temperature rise on the PDMS surface was negligible (less than 1 °C) after 1 h of illumination. Droplet volumes were measured using a 100 μL syringe and were recorded within a few minutes after being dispensed onto the surfaces. The concentration of **2** was determined with UV−vis by monitoring the disappearance of the absorption of 1 at 378 nm. The starting concentration of **1** was 0.20 mM.

Errors arise from 3 main sources. (1) Volumes were recorded by drawing the water droplet up into a 100 μL Hamilton syringe, which introduced a bubble into the dead space of the syringe barrel and plunger producing ±2 μL resolution; this equates to errors ranging from 2% for the 100 μL droplet to 20% for the 10 μL droplet. (2) The absorbance of the droplet was measured, and the concentration of **1** was calculated using its absorption coefficient and reference to a calibration curve (accuracy is ±0.1%). Droplets larger than 25 μL were removed from the surface and placed into a 100 μL quartz cuvette, whereas droplets ≤25 μL were diluted to 100 μL with H_2O and the concentration of **1** was back-calculated. Both experiments used a 1 cm path length. (3) Droplet evaporation introduced a volumetric error that ranged from a high of 60% for the 10 μL droplet to a low of 5% for the 100 μL droplet. The errors introduced by (1) and (2) were usually smaller relative to the error introduced by the droplet evaporation in (3), which is most significant for the smaller droplets.

■ ASSOCIATED CONTENT

Supporting Information

Images of surface A with water droplets of various volumes and the silicon *Pc* glass prior to grinding. Plots of the anthracene **1** photooxidation are provided with the data fitted to first-order kinetic reactions as well as tables for the calculation of the number of posts contacting the water droplets. This information is available free of charge via the Internet at http://pubs.acs.org.

■ AUTHOR INFORMATION

Corresponding Author

daebisher@shorter.edu; alan.lyons@csi.cuny.edu; agreer@brooklyn.cuny.edu

Notes

The authors declare no competing financial interest.

■ ACKNOWLEDGMENTS

D.A. acknowledges support from the Department of Natural Sciences at Shorter University. D.B. and A.G. acknowledge support from the National Institute of General Medical Sciences (NIH SC1GM093830). Y.L., Y.Z., Q.F.X., and A.M.L. acknowledge support from the NYS Empire State Development's Division of Science, Technology & Innovation (NYSTAR). We also thank Alison Domzalski for the photography work and Leda Lee for the graphic arts work.

■ REFERENCES

(1) Clennan, E. L.; Pace, A. *Tetrahedron* **2005**, *61*, 6665−6691.
(2) Rebek, J., Jr.; Brown, D.; Zimmerman, S. *J. Am. Chem. Soc.* **1975**, *97*, 454−455.
(3) Rebek, J., Jr.; Gavina, F. *J. Am. Chem. Soc.* **1975**, *97*, 3453−3456.
(4) Rebek, J., Jr.; Brown, D.; Zimmerman, S. *J. Am. Chem. Soc.* **1975**, *97*, 4407−4408.
(5) Wolf, S.; Foote, C. S.; Rebek, J., Jr. *J. Am. Chem. Soc.* **1978**, *100*, 7770−7771.
(6) Roh, K.-H.; Martin, D. C.; Lahann, J. *J. Am. Chem. Soc.* **2006**, *128*, 6796−6797.
(7) Nakata, K.; Nishimoto, S.; Yuda, Y.; Ochiai, T.; Murakami, T.; Fujishima, A. *Langmuir* **2010**, *26*, 11628−11630.
(8) Nakajima, A.; Koizumi, S.; Watanabe, T.; Hashimoto, K. *Langmuir* **2000**, *16*, 7048−7050.
(9) Yoshida, N.; Takeuchi, M.; Okura, T.; Monma, H.; Wakamura, M.; Ohsaki, H.; Watanabe, T. *Thin Solid Films* **2006**, *502*, 108−111.
(10) Soliveri, G.; Annunziata, R.; Ardizzone, S.; Cappelletti, G.; Meroni, D. *J. Phys. Chem. C* **2012**, *116* (50), 26405−26413.
(11) Lai, Y.; Pan, F.; Xu, C.; Fuchs, H.; Chi, L. *Adv. Mater.* **2013**, *25*, 1682−1686.
(12) Feng, X.; Zhai, J.; Jiang, L. *Angew. Chem., Int. Ed.* **2005**, *44*, 5115−5518.
(13) Sun, W.; Zhou, S.; Chen, P.; Peng, L. *Chem. Commun.* **2008**, 603−605.
(14) Xu, Q.; Liu, Y.; Lin, F.; Mondal, B.; Lyons, A. M. *ACS Appl. Mater. Interfaces* **2013**, *5*, 8915−8924.
(15) Stepien, M.; Saarinen, J. J.; Teisala, H.; Tuominen, M.; Aromaa, M.; Haapanen, J.; Kuusipalo, J.; Mäkelä, J. M.; Toivakka, M. *Langmuir* **2013**, *29*, 3780−3790.
(16) Crick, C. R.; Bear, J. C.; Kafizas, A.; Parkin, I. P. *Adv. Mater.* **2012**, *24*, 3505−3508.
(17) Rolland, J. P.; Van Dam, R. M.; Schorzman, D. A.; Quake, S. R.; DeSimone, J. M. J. *Am. Chem. Soc.* **2004**, *126*, 2322−2323.
(18) Shim, J.-U.; Olguin, L. F.; Whyte, G.; Scott, D.; Babtie, A.; Abell, C.; Huck, W. T. S.; Hollfelder, F. *J. Am. Chem. Soc.* **2009**, *131*, 15251−15256.
(19) Hatakeyama, T.; Chen, D. L.; Ismagilov, R. F. *J. Am. Chem. Soc.* **2006**, *128*, 2518−2519.
(20) Lemke, E. A.; Gambin, Y.; Vandelinder, V.; Brustad, E. M.; Liu, H.-W.; Schultz, P. G.; Groisman, A.; Deniz, A. A. *J. Am. Chem. Soc.* **2009**, *131*, 13610−13612.
(21) Zheng, Z.; Azzaroni, O.; Zhou, F.; Huck, W. T. S. *J. Am. Chem. Soc.* **2006**, *128*, 7730−7731.
(22) Barahman, M.; Lyons, A. M. *Langmuir* **2011**, *27*, 9902−9909.
(23) Bartusik, D.; Aebisher, D.; Ghafari, B.; Lyons, A. M.; Greer, A. *Langmuir* **2012**, *28*, 3053−3060.
(24) Cassie, A. B. D.; Baxter, S. *Trans. Faraday Soc.* **1944**, *40*, 546−551.
(25) Gerdes, S.; Cazabat, A. M.; Ström, G.; Tiberg, F. *Langmuir* **1998**, *14*, 7052−7057.
(26) Chandra, D.; Yang, S. *Langmuir* **2011**, *27*, 13401−13405.
(27) Lv, C.; Hao, P. *Langmuir* **2012**, *28*, 16958−16965.
(28) McHale, G.; Aqil, S.; Shirtcliffe, N. J.; Newton, M. I.; Erbil, H. Y. *Langmuir* **2005**, *21*, 11053−11060.
(29) Ghasemi, H.; Ward, C. A. *J. Phys. Chem. C* **2010**, *114*, 5088−5100.
(30) Fang, G.; Li, W.; Wang, X.; Qiao, G. *Langmuir* **2008**, *24*, 11651−11660.
(31) Hao, P.; Lv, C.; Yao, Z. *Langmuir* **2013**, *29*, 5160−5166.
(32) Cheng, D. F.; Urata, C.; Masheder, B.; Hozumi, A. *J. Am. Chem. Soc.* **2012**, *134*, 10191−10199.
(33) Ling, Y. L.; Ng, T. W.; Neild, A. *Langmuir* **2010**, *26*, 17695−17702.
(34) Lindig, B. A.; Rodgers, M. A. J.; Schaap, A. P. *J. Am. Chem. Soc.* **1980**, *102*, 5590−5593.
(35) Davies, H. M. L.; Walji, A. M.; Nagashima, T. *J. Am. Chem. Soc.* **2004**, *126*, 4271−4280.
(36) Davies, I. W.; Matty, L.; Hughes, D. L.; Reider, P. J. *J. Am. Chem. Soc.* **2001**, *123*, 10139−10140.
(37) Skovsen, E.; Snyder, J. W.; Lambert, J. D.; Ogilby, P. R. *J. Phys. Chem. B* **2005**, *109* (18), 8570−8573.
(38) Lindig, B. A.; Rodgers, M. A. *Photochem. Photobiol.* **1981**, *33*, 627−634.
(39) Haag, W. R.; Hoigné, J. *Environ. Sci. Technol.* **1986**, *20* (4), 341−348.

(40) Jensen, R. L.; Arnbjerg, J.; Ogilby, P. R. *J. Am. Chem. Soc.* **2012**, *134*, 9820−9826.
(41) Jensen, R. L.; Arnbjerg, J.; Birkedal, H.; Ogilby, P. R. *J. Am. Chem. Soc.* **2011**, *133*, 7166−7173.
(42) Ruiz-González, R.; Cortajarena, A. L.; Mejias, S. H.; Agut, M.; Nonell, S.; Flors, C. *J. Am. Chem. Soc.* **2013**, *135*, 9564−9567.
(43) Chin, K. K.; Trevithick-Sutton, C. C.; McCallum, J.; Jockusch, S.; Turro, N. J.; Scaiano, J. C.; Foote, C. S.; Garcia-Garibay, M. A. *J. Am. Chem. Soc.* **2008**, *130*, 6912−6913.
(44) Liu, H.-W.; Ngo, A. T.; Cosa, G. *J. Am. Chem. Soc.* **2012**, *134*, 1648−1652.
(45) Naito, K.; Tachikawa, T.; Cui, S.-C.; Sugimoto, A.; Fujitsuka, M.; Majima, T. *J. Am. Chem. Soc.* **2006**, *128*, 16430−16431.
(46) Naito, K.; Tachikawa, T.; Fujitsuka, M.; Majima, T. *J. Phys. Chem. C* **2008**, *112*, 1048−1059.
(47) Fudickar, W.; Fery, A.; Linker, T. *J. Am. Chem. Soc.* **2005**, *127*, 9386−9387.
(48) Bartusik, D.; Aebisher, D.; Lyons, A. M.; Greer, A. *Environ. Sci. Technol.* **2012**, *46*, 12098−12104.
(49) Zhao, Y.; Li, H.; Zeng, X. *J. Am. Chem. Soc.* **2013**, *135*, 15549−15558.
(50) Levesque, F.; Seeberger, P. H. *Org. Lett.* **2011**, *13*, 5008−5011.
(51) Pessoni, L.; Lacombe, S.; Billon, L.; Brown, R.; Save, M. *Langmuir* **2013**, *29*, 10264−10271.
(52) Yavorskyy, A.; Shvydkiv, O.; Nolan, K.; Delauré, Y. M. C.; Oelgemöller, M. *Green Chem.* **2012**, *14*, 888−892.